Using Rotation Curves to Assess the Viability of Warm and Cold Dark Matter Profiles

Ben Taylor

School of Physics and Astronomy

University of Southampton

19th April, 2018

Abstract

In this paper we assess five profiles for dark matter halos, the NFW and DC14 profiles for cold dark matter and three profiles for warm dark matter. We plot the M_{halo}-c and M_{halo}-M_{star} relations, the baryonic Tully-Fisher relation and the baryonic-total radial acceleration relation as well as looking at the reduced chi squared values for each dark matter model. We then further compare the models by re-examining these plots after imposing priors based on ΛCDM predictions. Ultimately we find that although the results for warm dark matter are promising we didn't have enough data from very low mass galaxies to come to a definitive conclusion about the viability of warm dark matter as an alternative to cold dark matter.

1 Introduction

Dark matter is currently theorized to constitute 26% of the mass-energy content of the universe, with another 69% being dark energy and just a 5% contribution from baryonic matter (Planck collab., 2016). Despite this it remains one of the biggest mysteries in modern day astronomy. It was first theorized in 1932 as a way to explain the discrepancy between the calculated gravitational mass of galaxy clusters derived from the virial theorem and the observed mass of the baryonic matter (Zwicky, 1933). Since then evidence has continued to reaffirm the existence of dark matter, and various theories have been put forward to suggest its properties and composition.

The most popular model for dark matter is currently the cold dark matter model, which works well for large scale galaxies; however at small scales (halo masses of $<10^9$ $M_\odot$) various problems arise and in this paper we look to warm dark matter models to attempt to resolve one of these problems, which involves the cores of small galaxies having a higher density of dark matter than what the cold dark matter models predict.

The models we examine in this paper for the density profiles of dark matter halos are the Navarro-Frenk-White profile (Navarro et al., 1996) and the DC14 profile (Di Cintio et al., 2014), which are both cold dark matter models, then three different models for warm dark matter. We use the SPARC (Spitzer Photometry & Accurate Rotation Curves) data set (Lelli et al., 2016) to attain values for the rotation curves of 127 different galaxies, then model the dark matter in the galaxies using our five models, before comparing the models and assessing their viabilities using a variety of different metrics, paying particular attention to the low mass galaxies.

2 An Overview of Dark Matter

2.1 Evidence For Dark Matter

The evidence that first caused the theory of dark matter to be postulated was when Fritz Zwicky used the virial theorem to calculate the mass of the Coma cluster of galaxies, and found that the cluster did not have enough visible mass to keep itself gravitationally bound. He therefore theorized that there must be more, unseen matter holding the cluster together.

The next major evidence for the existence of dark matter was in the 1960's in the form of the rotation curves of galaxies (Rubin, Thonnard and Ford, 1980). By observing the rotation curves of different galaxies we see that although the velocities towards the centre match up with the

expectations we have from theoretical calculations using Newtonian physics; as we measure the velocities further from the centre, we would expect them to drop off after reaching a peak. However, what we observe is a flat rotation curve that does not drop off, as seen in figure 1 for the Andromeda galaxy. From this flattening of the rotation curve we can infer that there is extra mass in the galaxy that remains unseen or "dark", and in fact if this is true then the majority of the galaxies mass must be comprised of this dark matter.

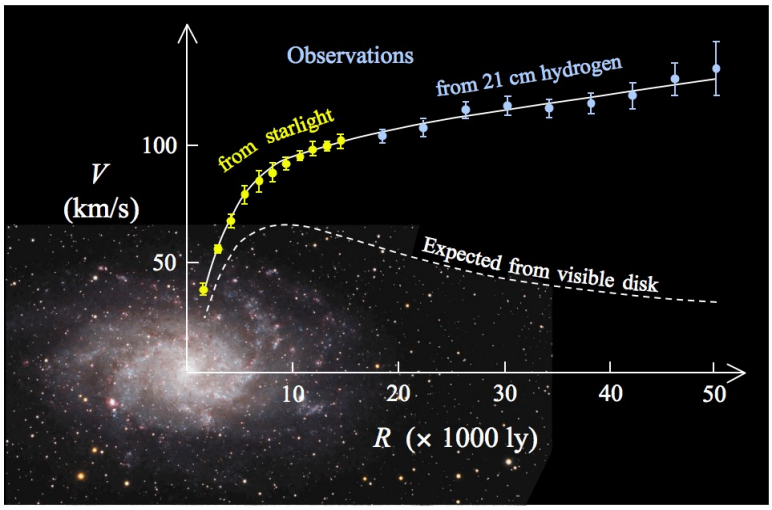

Figure 1 - Diagram Illustrating the observed rotation curve of M33 (Andromeda), and the expected curve using only baryonic matter. Public domain image taken from https://en.wikipedia.org/wiki/Galaxy_rotation_curve

From these discrepancies we can then create a density profile for the amount and distribution of extra mass in the galaxy so that our theoretical predications match up with the observed rotation curves. This is what we attempt to do in this paper using a numerical simulation and the SPARC data set.

Aside from these there are many other pieces of evidence that point towards the existence of dark matter. When we look at the velocities of individual galaxies travelling within a galaxy cluster we see similar effects to the rotation curves within the galaxies themselves i.e. our observations can only match up with our current understanding of Newtonian physics by adding extra mass to the clusters. Another thing we observe from galaxy clusters and superclusters is gravitational lensing. Gravitational lensing is a visual effect we observe due to light bending around huge masses, such as clusters of galaxies, as it travels to us, shown in figure 2. From the magnitude of the effect we can calculate the mass of the object causing the gravitational lens, and once again we find that our calculations infer that there is much more mass present than what we would expect from baryonic matter.

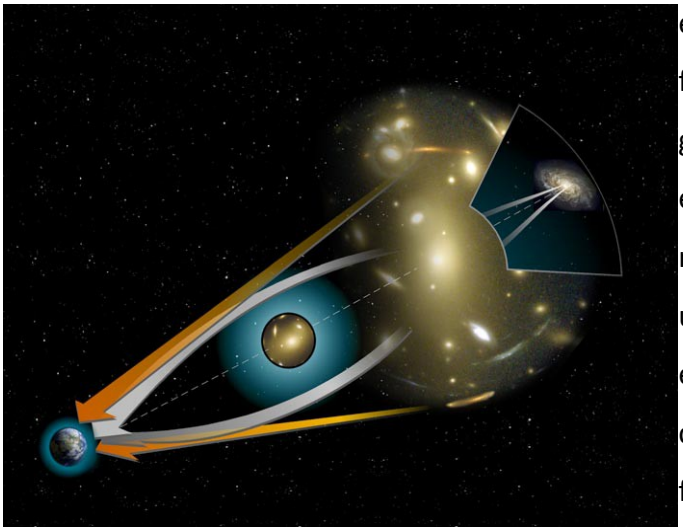

Figure 2 - Diagram illustrating light bending due to the effects of gravitational lensing. Public Domain image taken from https://en.wikipedia.org/wiki/Gravitational_lens.

Finally, another argument for dark matter is the structure of the universe itself. When galaxies were first formed, in the early universe it was dues to differences in the density of matter, which then collapsed to form stars and galaxies. However, the early universe was radiation dominant, which would have affected the baryonic matter and washed out the differences in density, meaning there would not have been enough time between the big bang and the present day to form the current structure of galaxies. However, dark matter is unaffected by radiation and provides a way to speed up the collapse of baryonic matter in time to see the galaxy structure we see today.

Although there are many observations that point to the existence of dark matter, there are still alternate theories that attempt to explain the evidence without the need for extra mass. The most popular of these theories is MOND (Modified Newtonian Dynamics) which suggests that our understanding of classical Newtonian mechanics is incomplete, and changes under very small accelerations, such as those on the outer rim of a galaxy. However, although these MOND theories do well at explaining rotation curves and the motions of galaxies, they fail to explain the formation of galaxies and no-one has been able to propose a satisfactory cosmological model using it, and it struggles to explain gravitational lensing.

2.2 Candidates for Dark Matter

There have been many proposed candidates for what could constitute dark matter since it was first theorized, a lot of which have been mostly disproved, and others which have shown more promise. They mostly fall into three categories: hot, warm and cold dark matter. The category a candidate falls into depends on its free-streaming length in the early universe with respect to the length of a protogalaxy. Particles with free-streaming lengths much larger than a protogalaxy fall into hot dark matter, those with a free-streaming length much smaller than a protogalaxy fall into cold dark matter, and those with a similar free-streaming length to a protogalaxy fall into warm dark matter.

Although a popular theory in the 1980's, hot dark matter candidates are to longer thought to contribute a significant portion of dark matter. Their free-streaming lengths in the early universe would imply that huge supercluster size objects formed first, before fragmenting into the galaxy structure observed today (this is known as “top-down” formation), whereas we know from deep-field observation that galaxies formed first, then clumped together to form clusters and

superclusters (a “bottom-up” formation) (Bertone, Hooper and Silk, 2005). From this we can assume that any hot dark matter candidates form only a small portion of dark matter. The neutrino is the most well known example of a hot dark matter particle.

Cold dark matter is the most widely accepted theory for dark matter, as it predicts bottom-up galaxy formation, which is what we have observed. However, problems arise with current pure CDM models when looking at dwarf galaxies, which will be discussed in more detail in section 2.3. It was once thought that dark matter could be made of MACHOs (Massive Compact Halo Objects) which are made of ordinary baryonic matter that we are unable to detect, such as black holes, brown dwarfs and neutron stars. However, these MACHOs are only thought to make up, at most, 20% of a dark matter halo, with the majority being made up of undiscovered particles (Alcock et al., 2000). The most popular examples of theorized particles for dark matters composition are the lightest particle predicted by supersymmetry, and axions (theoretical particles used to explain phenomenon in quantum chromodynamics). The NFW and DC14 profiles that we will be looking at in this paper are both based on cold dark matter.

We will also be looking at three different models of warm dark matter. Warm dark matter refers to dark matter candidates which have free-streaming lengths in-between those of hot dark matter and cold dark matter. Sterile neutrinos and gravitinos are two examples are warm dark matter particles.

2.3 Problems with CDM models at small scales

Three major problems arise when looking at CDM models: the missing satellites problem, the cusp-core problem and the too-big-to-fail problem.

In the Local Group we can observe roughly 50 satellite galaxies within the virial radius of the Milky Way (Bullock and Boylan-Kolchin, 2017). This is far below the number of dark matter halos we would expect to have formed under a cold dark matter model (over 1000). Although it is likely that there are some very faint galaxies in the Local Group which have yet to be discovered, it is extremely unlikely that these will make up the predicted number of halos. A way to resolve this problem could be to assume that as dark matter halos become less massive they become increasingly inefficient at forming galaxies, therefore the low number of satellite galaxies we observe is due to the very low mass halos not having a very high chance to form a galaxy.

When we simulate galaxy formation around the Milky Way using a CDM model, we find that the predicted mass of the most massive subhalos is higher than the most massive satellite galaxies we observe in the Local Group (Bullock and Boylan-Kolchin, 2017). This goes against abundance matching, the prediction that the more massive the dark matter halo of a galaxy, the more higher the total mass of the stars in the galaxy will be. In the missing satellites problem, the assumption was that the lower mass halos were less efficient at forming galaxies, however if these predicted massive subhalos exist they should be too-big-to-fail i.e. since they are so massive, galaxy formation should be guaranteed. This is the too-big-to-fail problem.

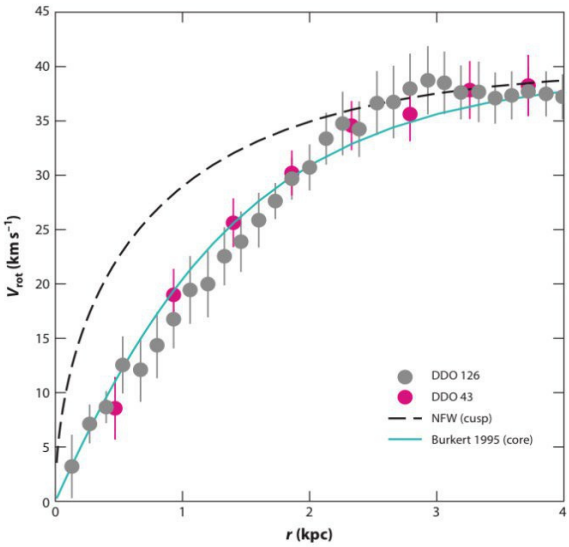

Figure 3 - The cusp-core problem. The dashed line is what we expect from models, the grey and pink data points are the actual data. Image from (Bullock and Boylan-Kolchin, 2017).

The final problem is the cusp-core problem. The problem here lies in the density profile of the dark matter in dwarf galaxies. As shown in figure 3, a cold dark matter model (the NFW model has been used for this example) predicts a much denser core than observations would suggest and a faster rising curve (or more "cuspy"). This is the problem we will be looking to solve in this paper. Although the NFW profile fails to provide an adequate model for these dwarf galaxies, the DC14 model has already proven itself to be a much more reliable model for these galaxies (Katz et al., 2016) and we will be looking at how well warm dark matter models solve this problem.

3 Modelling the Dark Matter

In order to model the dark matter contained in the galaxies in our data sample, we took the different velocity components in each galaxy (disk velocity, bulge velocity, gas velocity and total velocity) and attempted to find the dark matter distribution which best fit the data. We had three parameters for each dark matter model, which we varied to find the best fit. These were the dark matter halo mass, the concentration parameter, which we will define in the next section, and the stellar mass-to-light ratio. An example of one of these fits is shown in figure 4.

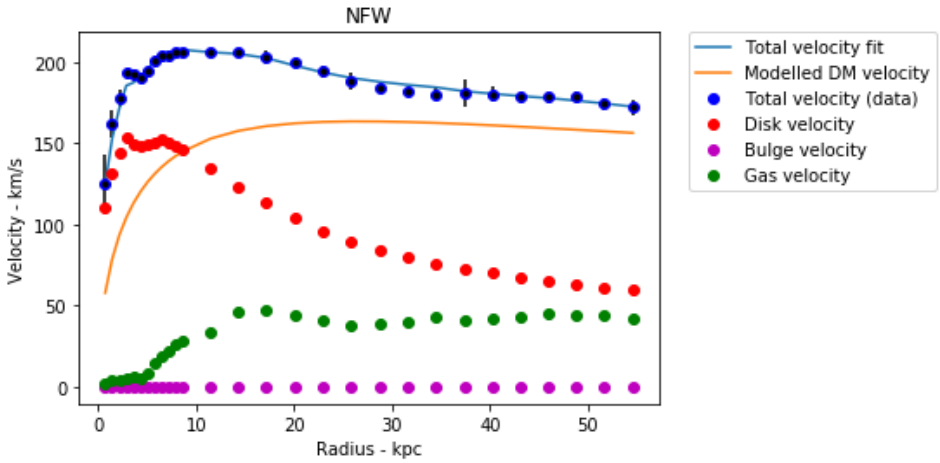

Figure 4 - The rotation curve of NGC5055 fit using the NFW halo model.

3.1 The NFW Profile

The density of the dark matter halos in the NFW profile is given by

$$\rho(r)=\frac{\rho_0}{\frac{r}{R_s}\left(1+\frac{r}{R_s}\right)^2} \tag{1}$$

where ρ_0 (the scale density) and R_s (the scale radius) are parameters which vary from halo to halo. The mass of the halo, M, within a certain radius, r, is therefore given by

$$M=\int_0^r 4\pi r^2 \rho(r)\,dr=4\pi\rho_0 R_s^3\left[\ln\left(\frac{R_s+r}{R_s}\right)-\frac{r}{R_s+r}\right] \tag{2}$$

We define the distance to edge of the halo as the viral radius, R_{vir}, which is the radius of the halo, assuming spherical symmetry, at which its density is 200 times the critical density of the universe. For this calculation we assume that $H_0 = 70$ km s^{-1} Mpc^{-1}. We can then introduce the concentration parameter, and define it as

$$R_{vir}=c\,R_s \tag{3}$$

In this case the total mass of the halo, M_{vir}, is

$$M_{vir}=\int_0^{R_{vir}} 4\pi r^2 \rho(r)\,dr=4\pi\rho_0 R_s^3\left[\ln(1+c)-\frac{c}{1+c}\right] \tag{4}$$

Given equations (2) and (4) and substituting in equation (3) to remove R_s, we can then find the mass within a certain radius, r, of a halo if given its mass, M_{vir}, and concentration, c.

3.2 The DC14 Profile

In the DC14 profile the density profile of the dark matter is given by

$$\rho(r)=\frac{\rho_0}{\left(\frac{r}{R_s}\right)^{\gamma}\left[1+\left(\frac{r}{R_s}\right)^{\alpha}\right]^{(\beta-\gamma)/\alpha}} \tag{5}$$

where -γ and -β are the inner and outer logarithmic slopes respectively, and α describes the transition between the two. These values are given by

$$\begin{aligned}\alpha&=2.94-\log_{10}[(10^{X+2.33})^{-1.08}+(10^{X+2.33})^{2.29}]\\ \beta&=4.23+1.34X+0.26X^2\\ \gamma&=-0.06-\log_{10}[(10^{X+2.56})^{-0.68}+(10^{X+2.56})]\end{aligned} \tag{6}$$

where $X = \log_{10}(M_*/M_{Halo})$. The concentration parameter is given by

$$c=\frac{R_{vir}}{r_{-2}} \tag{7}$$

where r_{-2} is the radius at which the logarithmic slope of the density profile is -2 and is given by

$$r_{-2}=\left(\frac{2-\gamma}{\beta-2}\right)^{1/\alpha} r_s \tag{8}$$

Since the NFW and DC14 profiles have different inner slopes, the NFW concentration is different to the DC14 concentration. We can convert between these values using the following relation

$$c_{NFW}=\frac{c_{DC14}}{1.0+e^{0.00001[3.4(X+4.5)]}} \tag{9}$$

Note that we use the value of 0.00001 suggested in (Katz et al., 2016) rather than the original 0.00003 provided in (Di Cintio et al., 2014) as we also found it provided better fits to the data. Using these equations we can use a similar method to the NFW model to calculate the halo mass within a particular radius, since the DC14 model is a version of the NFW model where α, β and γ vary as a function of the stellar to halo mass ratio. In the NFW model these values are (α, β, γ) = (1, 3, 1).

The simulations used to derive the DC14 model neglect the effects of supermassive black holes, therefore the simulations are only likely to be accurate up to halo masses of 10^{12} solar masses. Also this model is only accurate for values of X from $-4.1 < X < -1.$, we therefore set a maximum value of X = -1.3 and a minimum value of X = -4.1 and and state that the model is extrapolated for galaxies outside of this range (Di Cintio et al., 2014).

The main difference between the NFW and DC14 profiles is the effects of baryons on the structure of dark matter halos (Di Cintio et al., 2014). While the NFW model is based off dark

matter only simulations, the DC14 model takes into account the effect of that baryons in the galaxies have on restructuring the dark matter halo by adopting variables in the density profile based on the stellar-dark matter mass ratio.

3.3 Warm Dark Matter Models

The warm dark matter models we used were for thermal warm dark matter with m = 3keV, and sterile neutrinos with m = 7keV and two different scattering angles of $\sin^2(2\theta) = 2\text{x}10^{-10}$ and $\sin^2(2\theta) = 5\text{x}10^{-11}$. For the models we used the same method as the NFW profile, and added in a restriction on c, making it a function of the halo mass based on data on the relation between M_{halo} and c (N. Menci, 2018, priv. comm.). While the cold dark matter models predict that the concentration of the halo will keep increasing as the halo mass gets lower, the warm dark matter models predict that the concentration will fall off at lower masses, peaking at just under $10^{11}\,M_\odot$. In order to better replicate values seen in nature for these parameters we imposed a random lognormal distribution on c with a standard deviation of 0.16 dex.

3.4 Fitting the rotation curves

After finding the mass of dark matter within a given radius, we can then use the equation

$$V = \sqrt{\frac{GM}{R}} \tag{10}$$

to calculate the velocity of the dark matter. We then combine this with the disk, bulge and gas velocities as follows

$$V_{tot}(r) = \sqrt{V_{dm}(r)^2 + V_{gas}(r)^2 + (M/L)\,V_{disk}(r)^2 + 1.4(M/L)\,V_{bulge}(r)^2} \tag{11}$$

In this equation we have used the approximate assumption that the stellar mass-to-light ratio of the bulge is 1.4 times the ratio of the disk (McGaugh, 2015).

When fitting the rotation curves we used very loose bounds for each parameter. The concentration parameter was allowed to vary from $1 < c < 100$ the halo mass was allowed to vary from $8 < \log_{10}(M_{Halo}/M_\odot) < 14$ and the stellar mass-to-light ratio was allowed to vary from a minimum of 0.02 and with the maximum value being calculated such that the combined stellar and gas velocity (equation (11) with V_{dm} set to 0) could not be higher than the total velocity.

4 Results

4.1 Goodness of fit of the rotation curves

In order to evaluate how well the modelled curves fit the data, we calculated the reduced chi squared values of each galaxy's rotation curve. The median χ_v^2 for each model were $\chi_v^2 = 1.44$ or NFW, $\chi_v^2 = 0.61$ for DC14, $\chi_v^2 = 2.36 \pm 0.07$ for WDM1, $\chi_v^2 = 2.36 \pm 0.09$ for WDM2 and $\chi_v^2 = 2.23 \pm 0.07$ for WDM3 (here, and for the remainder of the paper we will refer to thermal WDM with m = 3keV as WDM1, sterile neutrinos with m = 7keV and $\sin^2(2\theta) = 2\text{x}10^{-10}$ as WDM2 and sterile neutrinos with m = 7keV and $\sin^2(2\theta) = 5\text{x}10^{-11}$ as WDM3). Since we are using a random lognormal distribution for the warm dark matter models, we ran the simulation 10 times for each model and took the mean χ_v^2 value for each. The error shown represents a 95% confidence interval. These errors are not necessary for the cold dark matter models, since they do not have any random elements and therefore give the same results each time they are run. Figure 5 shows the cumulative distribution function of the χ_v^2 values for the galaxies. From these median values, and from the figure we can clearly see that the DC14 model provides by far the best fits for the galaxy sample we had, with over half of the galaxies in the sample having a χ_v^2 value of $\chi_v^2 < 1$, compared to ~40% for the NFW model and only a quarter of the galaxies for the warm dark matter models. We also see that the warm dark matter models performed significantly worse here, compared to the cold dark matter models. However, although this result clearly shows that the warm dark matter models do not provide as good χ_v^2 fits in our galaxy sample compared to the cold dark matter models, this is to be expected, considering that our models for warm dark matter are simply the NFW model with an extra restriction put in place over one of our parameters (the concentration). In order to properly evaluate the performance of warm dark matter models compared to cold dark matter models we must compare the values given by our simulations to the values predicted by the ΛCDM model.

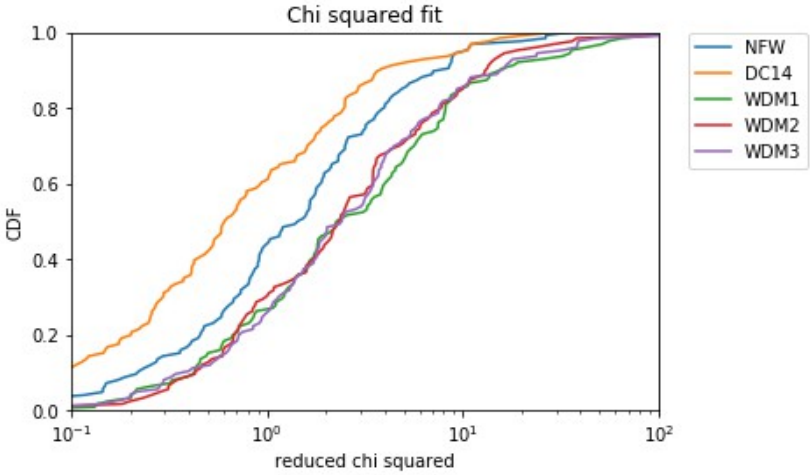

Figure 5 - Cumulative distribution function, plotted against the reduced chi squared values for each model.

4.2 Comparing values to ΛCDM predictions

The ΛCDM model makes various predictions about the parameters we have obtained in fitting the rotation curves. Therefore, since we have a large sample of galaxies to examine, we can compare the best fit parameters given by each model to these predictions, and use this as another means of evaluating their effectiveness.

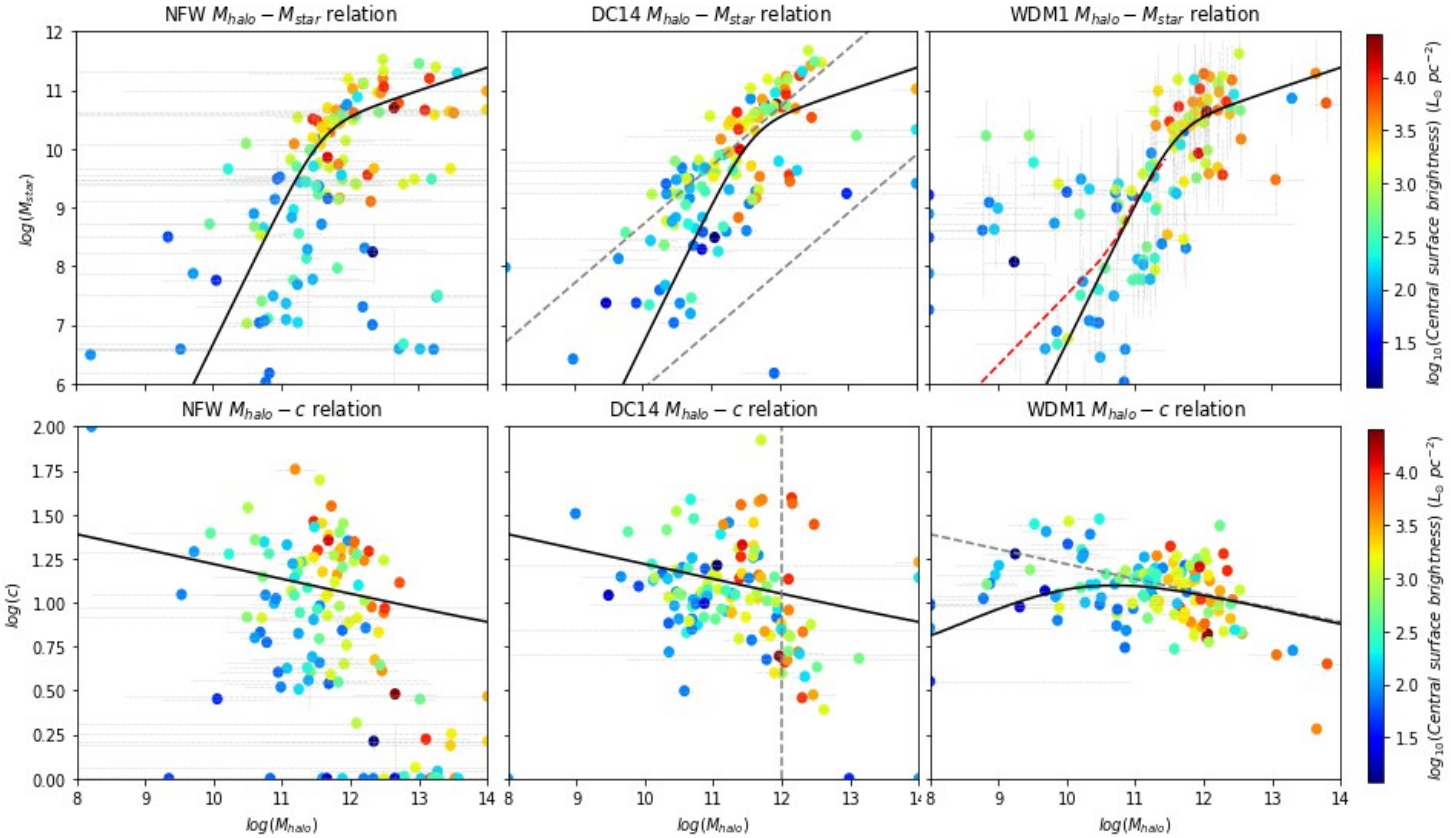

Figure 6 - The Mhalo-Mstar and Mhalo-c relations for the NFW, DC14 and WDM1 models. The solid black line in the top graphs are the predictions made by abundance matching (Moster et al., 2012). The dotted lines on the DC14 graph on the top represent X = -1.3 and X = -4.1. The red dotted line on WDM1 represents preliminary values for the Mhalo-Mstar relation for warm dark matter (Shankar et al., in prep). The solid black lines on the bottom graphs represent the expected Mhalo-c relation from (Schneider., 2015) for NFW and DC14 and (N. Menci, priv. comm.) for WDM1.

In Figure 6 you can see the relationships between stellar mass and halo mass on the top row, and halo mass and concentration on the bottom row. Note that due to the warm dark models being relatively similar, we have only included one WDM model in these plots. The plots for the remaining models can be found in appendix B. The M_{halo}-M_{star} relation is one we get from abundance matching (Moster et al., 2012) and the M_{halo}-c relation is from dark matter simulations (Schneider, 2015). From the NFW plot in the top left we can see that there is a lot of scatter, especially in galaxies with lower stellar mass, indicating that the best fit parameters for the NFW

model do not agree with abundance matching in galaxies with low stellar masses. This is a known shortcoming of the NFW model. As stated in (Katz et al., 2016) the DC14 model tends to provide much better fits for galaxies with low mass and low surface brightness. You can see this comparison for the low surface brightness galaxy, NGC3109, in figure 7. Another, related, problem with the NFW model is that it often grossly underestimates the concentration for galaxies with low surface brightnesses (Kuzio de Naray et al., 2009). This can be seen very clearly in our plot in the lower left of figure 6, where many of the LSB galaxies are along the very bottom of the graph, indicating a much lower concentration than simulations would suggest. We also see in this plot that the scatter around the predicted relation is quite large and it is hard to conclusively say whether or not these points follow the relation.

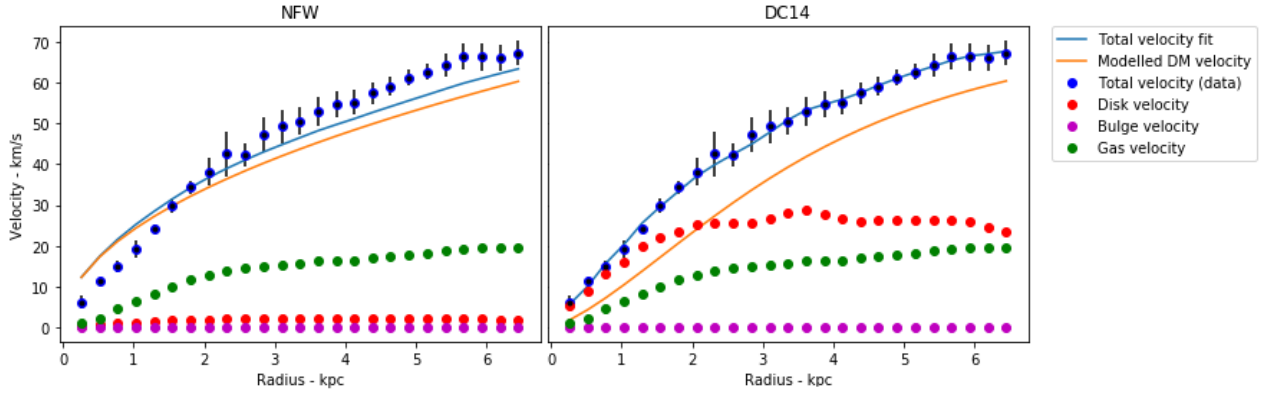

Figure 7 - Comparison of the NFW and DC14 models for the dark matter dominated, low mass galaxy, NGC3109.

Comparing the NFW and DC14 plots we find a sizeable improvement, as the scatter is greatly reduced for both plots, showing far fewer outliers, and the clump of galaxies with extremely low concentrations has almost disappeared. These values are much more in line with what we expect to see from abundance matching and dark matter simulations and although there are still some outliers, the DC14 model is a clear improvement over the NFW model when looking at this metric.

Turning our attention to the plots for warm dark matter we again see the scatter in the M_{halo}-M_{star} relation to be fairly low, and in line with the predictions made by abundance matching. The number of outliers, however is greater than what we see with the DC14 model, but less than in the NFW model. The M_{halo}-c relation for WDM has already been set in our WDM model when running the curve fitting, so it cannot be used to assess the WDM model any further.

Overall, in the metrics used so far the DC14 model has proven itself to be the best of the models used, although WDM seems to be an improvement over NFW when looking at abundance

matching.

The next metric we used to compare the models was the baryonic Tully-Fisher relation, which can be seen in figure 8. Here we plot the baryonic mass of the galaxies against the velocity at the maximum point on their rotation curves as suggested in (Ponomareva et al., 2017).

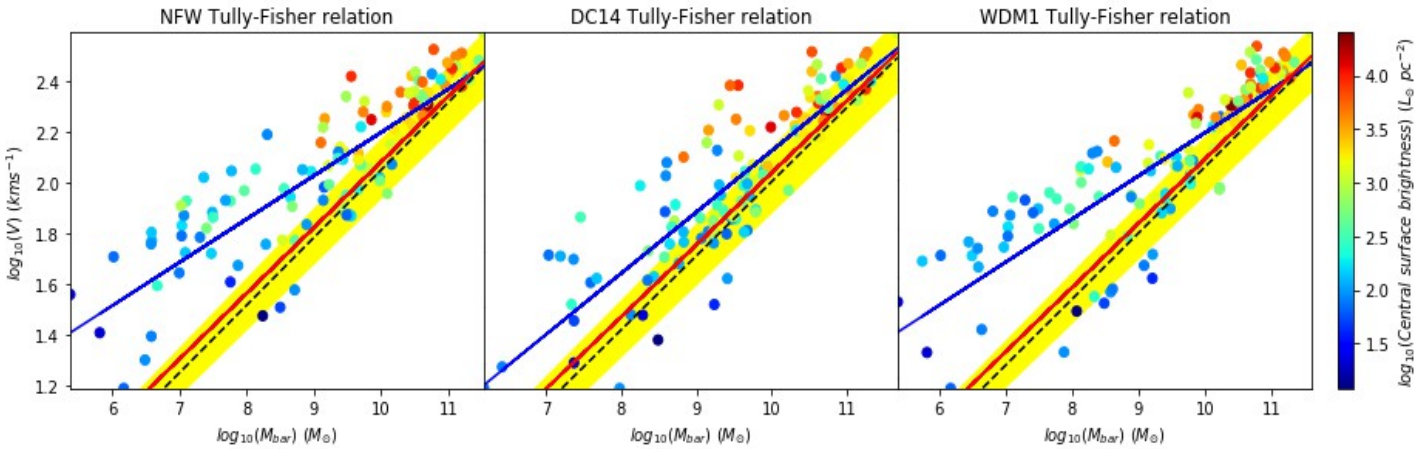

Figure 8 - The baryonic Tully-Fisher relation. The blue line represents our line of best fit, the red line is the observed data and the dashed line is the theoretical prediction, with the yellow space being one standard deviation (Ponomareva et al., 2017).

From these graphs we can see that all of the models seem to either overestimate the velocity of the rotation curves, or underestimate the baryonic mass, meaning a large portion of the galaxies lie to the left of the theoretical and observed data. However, looking at these plots it is clear that the DC14 model fits the observed data and theoretical predictions better than the other two models, which are similar. The reason for this could be partially that all the models are trying to fit the same curves, therefore all are attempting to fit the same maximum velocity, however as we have already seen the DC14 model is superior to the other models with regards to goodness of fits, meaning it is more likely to arrive at the correct value for velocity.

In figure 9 we look at plots of the maximum acceleration of the baryonic matter in a galaxy plotted against the maximum total acceleration in the galaxy. The theoretical predictions for this model made in (McGaugh et al., 2016) provide the acceleration scale parameter, g_s , which we can use to find the best matching g_s value for each of our models. The theory suggests that the expected value is $g_s = 1.20 \pm 0.02$ (random) ± 0.24 (systematic) $\times 10^{-10}$ ms^{-2}. For NFW we got a value of $g_s = 2.96 \times 10^{-10}$ ms^{-2}, for DC14 we got $g_s = 5.70 \times 10^{-11}$ ms^{-2}, for WDM1 $g_s = 2.20 \times 10^{-10}$ ms^{-2}, for WDM2 $g_s = 2.00 \times 10^{-10}$ ms^{-2}, for WDM3 $g_s = 1.93 \times 10^{-10}$ ms^{-2}. These results show that the warm dark matter models are the closest to theoretical predictions, with the NFW model being furthest

away. From the scatter plots we can see that all three models follow the relation fairly well, however there is noticeably more scatter on the NFW plot, and the DC14 plot also seems to have a little more scatter than the WDM models. This would indicate that warm dark matter could potentially provide an improvement over the cold dark matter models when looking at the accelerations within galaxies.

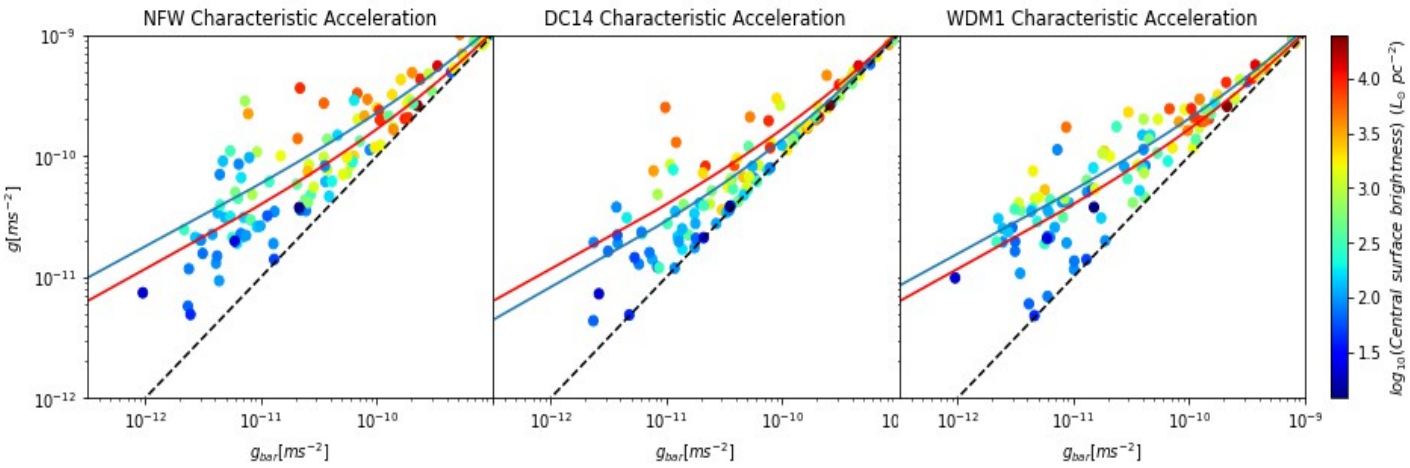

Figure 9 - The baryonic acceleration plotted against the total acceleration. The red line indicates the theoretical relation (McGaugh et al., 2016), and the blue line is our line of best fit for the data.

4.3 Imposing priors based on ΛCDM predictions

To further test our models we next imposed restrictions on the parameters of our curve fitting based on the M_{halo}-M_{Star} relation given by abundance matching. Similarly to the warm dark matter M_{halo}-c relation we gave the relation a lognormal distribution with a standard deviation of 0.16 dex, which can be seen in figure 10 for both cold and warm dark matter.

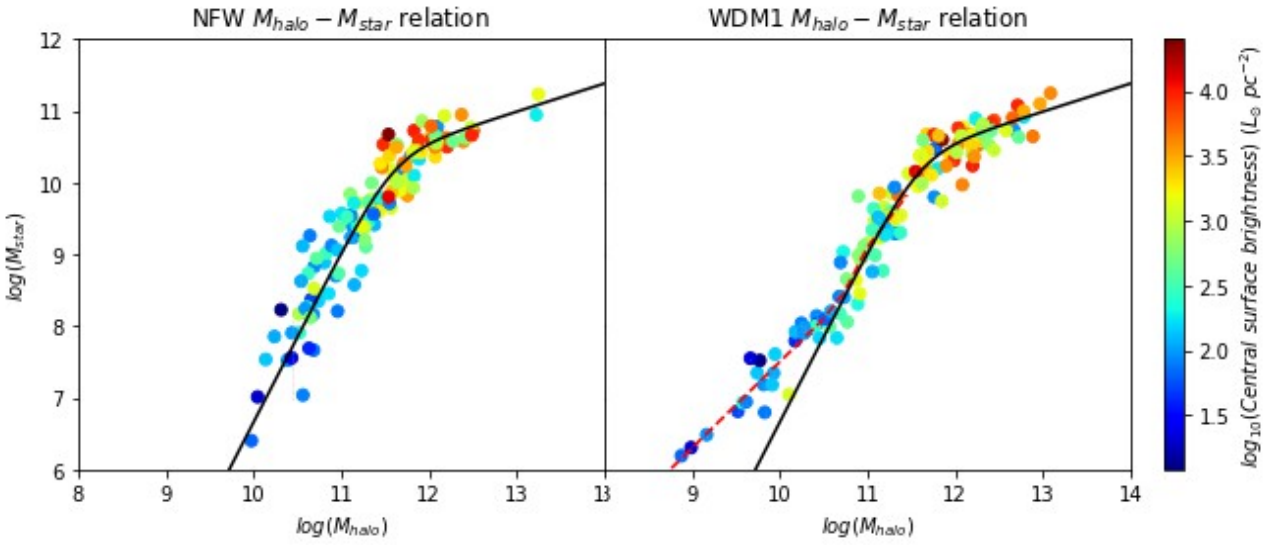

Figure 10 - The Halo mass- Stellar mass relation for NFW and WDM models with priors imposed

In figure 11 you can see how the concentrations in the NFW and DC14 models have changed after adding the priors (WDM is not included as the M_{halo}-c relation is pre-determined for those models). Neither have been affected significantly, however, it is noticeable that the clump of galaxies which had very low concentrations in the NFW model are no longer present, indicating that forcing these priors has resulted in some of the galaxies being fitted with more realistic concentration values.

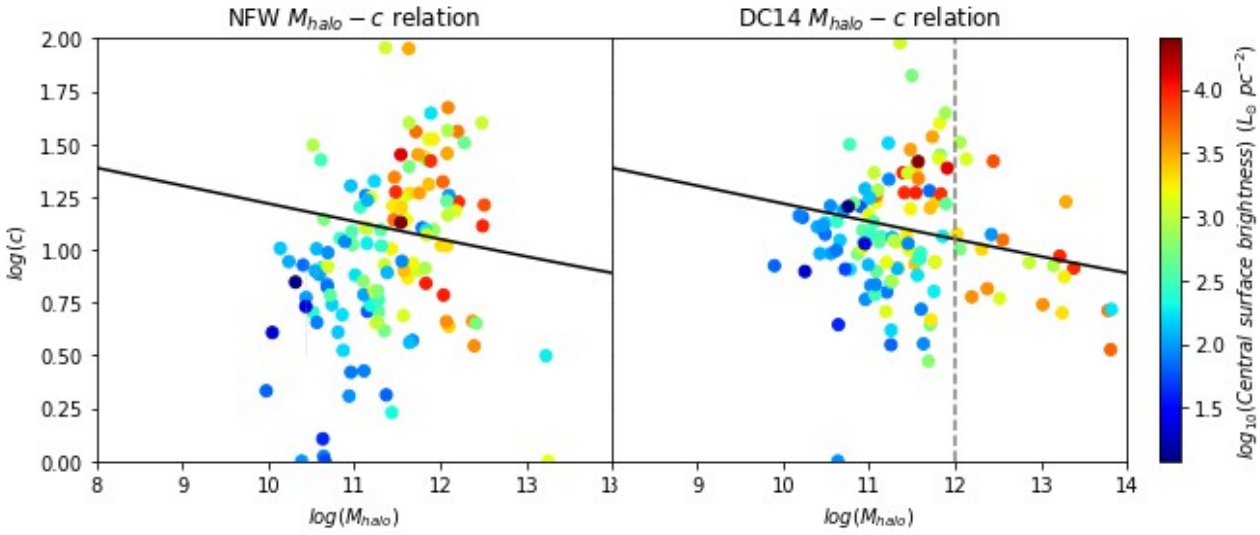

Figure 11 - The Halo mass-concentration relation for NFW and DC14 after imposing the priors

The median reduced chi squared values we obtained with the ΛCDM priors were $\chi_\nu^2 = 2.56$ for NFW, $\chi_\nu^2 = 2.61$ for DC14, $\chi_\nu^2 = 5.57$ for WDM1, $\chi_\nu^2 = 5.32$ for WDM2 and $\chi_\nu^2 = 4.79$ for WDM3. The values plotted against the cumulative distribution function can be seen in figure 12. The values for all models have decreased, when compared to our previous results, however this is to be expected when imposing new restrictions on our parameters. The WDM models still have worse fits than the other models, even with these priors imposed, however, surprisingly the priors have affected the DC14 model much more than the NFW model, making them roughly on par with one another.

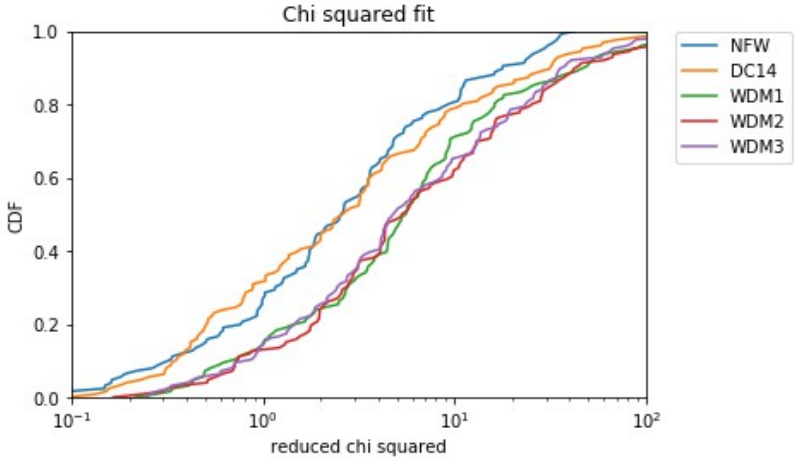

Figure 12 - Reduced Chi Squared values with ΛCDM priors imposed

Looking at figure 13 we can see that the priors have produced a very noticeable improvement on the baryonic Tully-Fisher relation. All of the models have performed reasonably well here, however the WDM models seem to have some form of systematic error, pushing the lower mass galaxies above the line which represents the observed data, and the theoretical predictions. The WDM model also seems to have slightly less scatter than the other two models. The reason for the improvement under the priors could be because they force the galaxies to have more sensible values for the stellar mass-to-light ratio, meaning the figures for baryonic mass are more accurate.

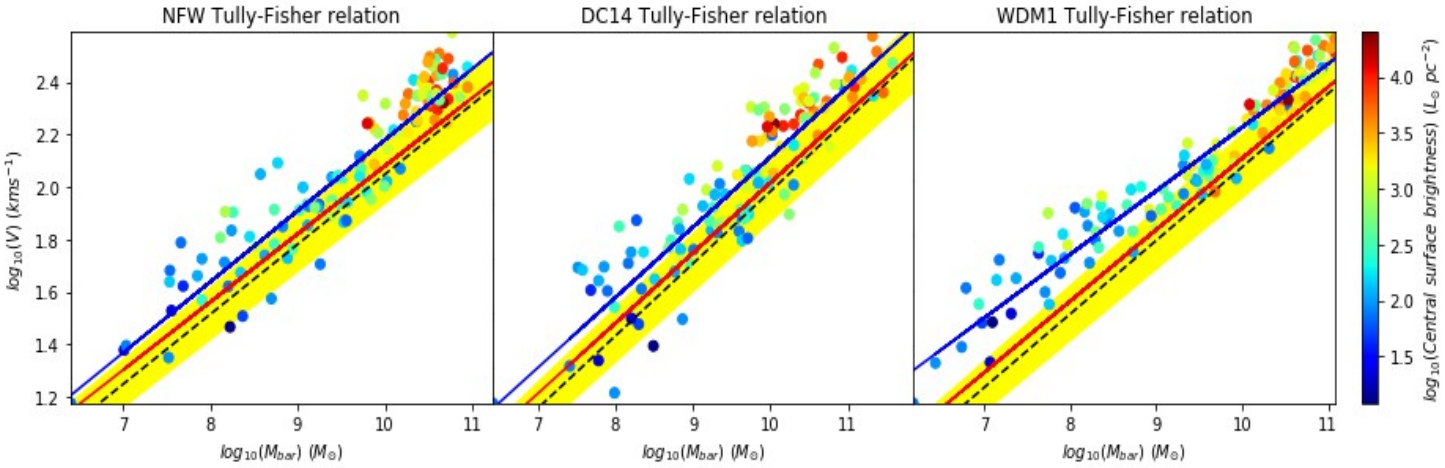

Figure 13 - Baryonic Tully-Fisher relation with ΛCDM imposed priors

From the acceleration relation with the imposed priors in figure 14, we see reduced scatter in all models. However, the NFW model does not seem to fit the predicted relation very well and the program has even struggled to find a best fit line for it, with a value of $g_s = 6.28 \times 10^{-10}\,ms^{-2}$. The DC14 model sees an improved line of best fit, with $g_s = 7.77 \times 10^{-11}\,ms^{-2}$ but this plot has quite a bit of scatter above the line of best fit and shows a substantial amount of galaxies with very

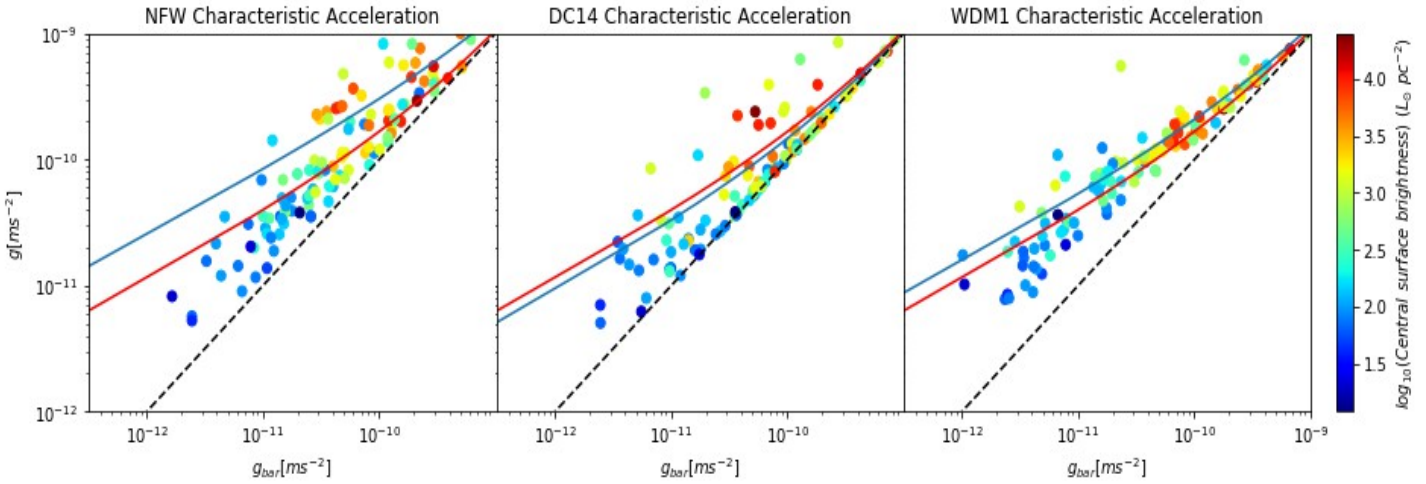

Figure 14 - The acceleration plots for each model with the ΛCDM priors imposed

similar, if not identical, values for total and baryonic acceleration, shown by the data points along the dotted line which should not be the case. The warm dark matter models however see greatly reduced scatter, with very few outliers, and notably the low surface brightness galaxies are close to the theoretical predictions, rather than the dotted line, as is the case with the DC14 model and to a certain extent, the NFW model. The values obtained were $g_s = 2.34 \times 10^{-10}$ ms^{-2} for WDM1, $g_s = 2.58 \times 10^{-10}$ ms^{-2} for WDM2 and $g_s = 2.35 \times 10^{-10}$ ms^{-2} for WDM3.

4.4 Comparing goodness of fit after imposing Further ΛCDM priors on the NFW and DC14 models

Up until this point in the paper there has been a slight imbalance in the way we have modelled cold dark matter vs warm dark matter. Namely, the concentration has been allowed to vary as a free parameter in the cold dark matter models, whereas it has always been a function of halo mass in the warm dark matter models. By imposing priors on the NFW and DC14 models similar to the ones used for warm dark matter we hope to more fairly compare the models.

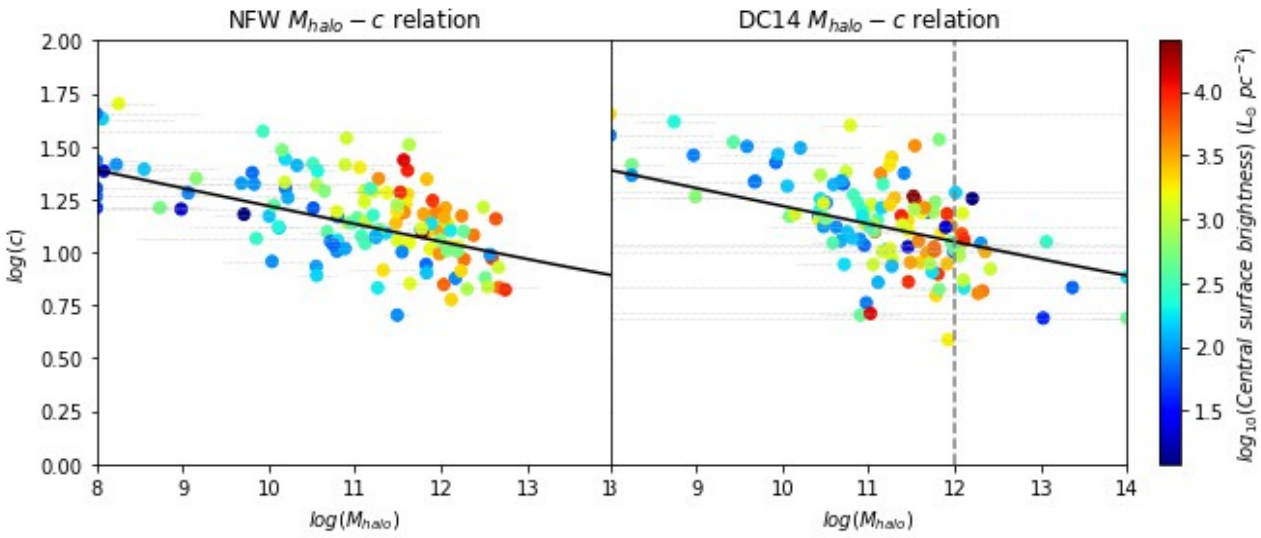

Figure 15 - Halo Mass-Concentration relation with ΛCDM priors imposed on concentration

In figure 15 you can see we have imposed priors on concentration similar to the ones imposed on warm dark matter i.e. a lognormal scatter with 0.16 dex standard distribution. Note that for now we have removed the previous sections priors.

If we now look at the χ_v^2 values for the NFW and DC14 models after imposing these priors we find that $\chi_v^2 = 2.73 \pm 0.11$ for NFW and $\chi_v^2 = 3.04 \pm 0.16$ for DC14. These values can be seen plotted against the cumulative distribution function in figure 16. These χ_v^2 values are noticeably worse than the values obtained for the warm dark matter models. Also, the difference is much bigger than it appears to be looking at these values, as the warm dark matter models only differ significantly from the NFW model at $<10^{10}$ solar masses, which is only true of a small number of the galaxies in our sample. This would indicate that the lower mass galaxies have much better fits using warm dark matter than cold dark matter.

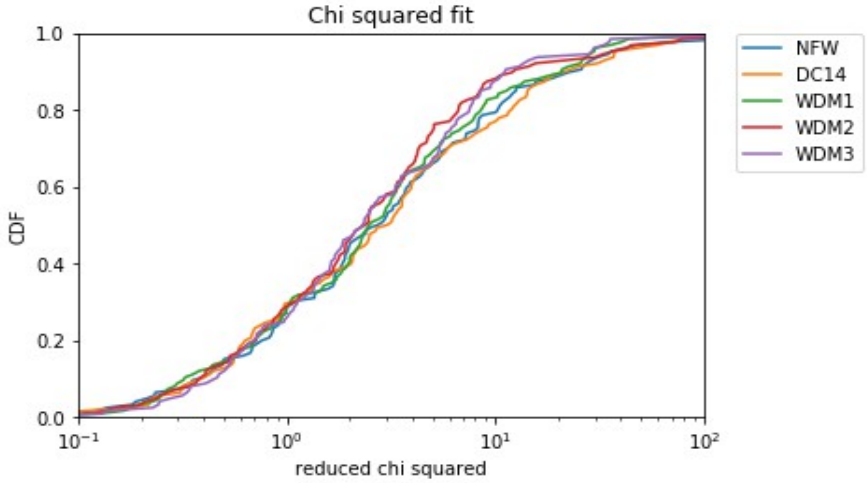

Figure 16 - Reduced chi squared values plotted against the cumulative distribution function with the NFW and DC14 concentration priors

Next, we will re-impose the abundance matching priors we had earlier and once again compare the χ_v^2 fits with the DC14 and NFW models with their new priors. Figure 17 shows the χ_v^2 plotted against the cumulative distribution function for these values. Our results were $\chi_v^2 = 5.84$ for NFW and $\chi_v^2 = 7.12$ for DC14. These results serve to reinforce the conclusions drawn above, that warm dark matter produces better fits for low mass galaxies when equivalent models are used.

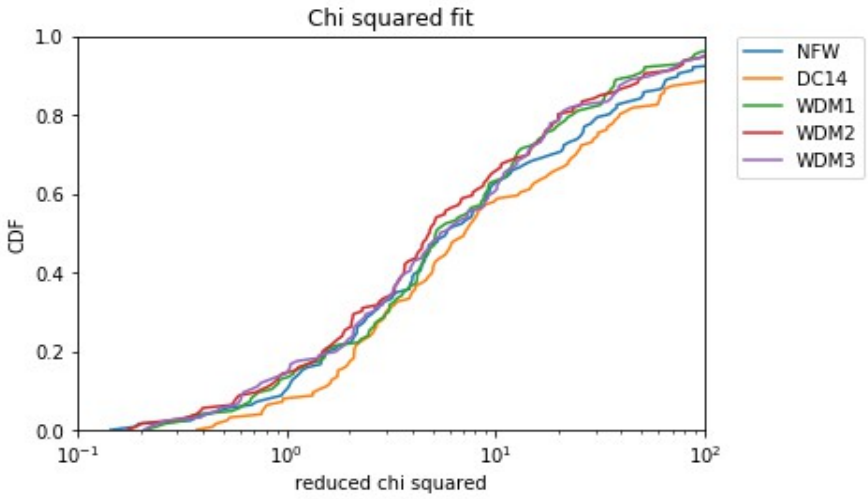

Figure 17 - Reduced chi squared values plotted against the cumulative distribution function with both the abundance matching priors and the NFW and DC14 concentration priors

Finally, in order to assess how much better the warm dark matter model is for low mass galaxies in this metric, we compiled a list of the 20 galaxies with the lowest found masses and looked at how good their fits were. Without abundance matching priors the medians were $\chi_v^2 = 2.49 \pm 0.34$ for NFW, $\chi_v^2 = 1.95 \pm 0.43$ for DC14, $\chi_v^2 = 1.85 \pm 0.04$ for WDM1, $\chi_v^2 = 1.88 \pm 0.06$ for WDM2 and $\chi_v^2 = 1.91 \pm 0.09$ for WDM3.

With the abundance matching priors we found $\chi_\nu^2 = 22.06 \pm 5.17$ for NFW, $\chi_\nu^2 = 8.53 \pm 1.78$ for DC14, $\chi_\nu^2 = 5.25 \pm 0.71$ for WDM1, $\chi_\nu^2 = 5.03 \pm 0.87$ for WDM2 and $\chi_\nu^2 = 5.62 \pm 0.63$ for WDM3. These results show that, the warm dark matter models do tend to provide better fits for low mass galaxies, especially when the ΛCDM priors based on abundance matching are applied. However, with the small sample of low mass galaxies we have data for, the extent of these differences cannot be conclusively stated.

5. Conclusions

In this paper we have used data for the rotation curves of 127 galaxies and attempted to model the dark matter they contain using the NFW and DC14 model, as well as three models for warm dark matter. We have found that for the majority of metrics we used to compare the models the DC14 model gave the best results, with the warm dark matter models generally performing slightly worse, although still better than the NFW model. When we imposed priors based on ΛCDM abundance matching predictions we found that the models were much more even, with the warm dark matter models generally having less scatter in their plots. Finally, when we imposed restrictions on the DC14 and NFW models similar to the ones already in place on the warm dark matter models we found that the warm dark matter models were able to better fit the curves than the NFW and DC14 models. This may indicate that the warm dark matter models are better at fitting the rotation curves in low mass galaxies than the NFW or DC14 models. However, since the main difference between the warm and cold dark matter models is in galaxies with low masses, it is hard to say this conclusively as we only had a small number of low mass galaxies in our sample.

More data, specifically in low mass galaxies will be required if we are to more effectively assess the viability of warm dark matter models as an alternative to cold dark matter.

References

Alcock, C., Allsman, R., Alves, D., Axelrod, T., Becker, A., Bennett, D., Cook, K., Dalal, N., Drake, A., Freeman, K., Geha, M., Griest, K., Lehner, M., Marshall, S., Minniti, D., Nelson, C., Peterson, B., Popowski, P., Pratt, M., Quinn, P., Stubbs, C., Sutherland, W., Tomaney, A., Vandehei, T. and Welch, D. (2000). The MACHO Project: Microlensing Results from 5.7 Years of Large Magellanic Cloud Observations. *The Astrophysical Journal*, 542(1), pp.281-307.

Bertone, G., Hooper, D. and Silk, J. (2005). Particle dark matter: evidence, candidates and constraints. *Physics Reports*, 405(5-6), pp.279-390.

Bullock, J. and Boylan-Kolchin, M. (2017). Small-Scale Challenges to the ΛCDM Paradigm. *Annual Review of Astronomy and Astrophysics*, 55(1), pp.343-387.

Di Cintio, A., Brook, C., Dutton, A., Macciò, A., Stinson, G. and Knebe, A. (2014). A mass-dependent density profile for dark matter haloes including the influence of galaxy formation. *Monthly Notices of the Royal Astronomical Society*, 441(4), pp.2986-2995.

Foreman-Mackey, D. (2016). corner.py: Scatterplot matrices in Python. *The Journal of Open Source Software*, 1(2), p.24.

Foreman-Mackey, D., Hogg, D., Lang, D. and Goodman, J. (2013). emcee: The MCMC Hammer. *Publications of the Astronomical Society of the Pacific*, 125(925), pp.306-312.

Katz, H., Lelli, F., McGaugh, S., Di Cintio, A., Brook, C. and Schombert, J. (2016). Testing feedback-modified dark matter haloes with galaxy rotation curves: estimation of halo parameters and consistency with ΛCDM scaling relations. *Monthly Notices of the Royal Astronomical Society*, 466(2), pp.1648-1668.

Kuzio de Naray, R., McGaugh, S. and Mihos, J. (2009). CONSTRAINING THE NFW POTENTIAL WITH OBSERVATIONS AND MODELING OF LOW SURFACE BRIGHTNESS GALAXY VELOCITY FIELDS. *The Astrophysical Journal*, 692(2), pp.1321-1332.

Lelli, F., McGaugh, S. and Schombert, J. (2016). SPARC: MASS MODELS FOR 175 DISK GALAXIES WITH SPITZER PHOTOMETRY AND ACCURATE ROTATION CURVES. *The Astronomical Journal*, 152(6), p.157.

McGaugh, S. (2015). THE SURFACE DENSITY PROFILE OF THE GALACTIC DISK FROM THE TERMINAL VELOCITY CURVE. *The Astrophysical Journal*, 816(1), p.42.

McGaugh, S., Lelli, F. and Schombert, J. (2016). Radial Acceleration Relation in Rotationally Supported Galaxies. *Physical Review Letters*, 117(20).

Moster, B., Naab, T. and White, S. (2012). Galactic star formation and accretion histories from matching galaxies to dark matter haloes. *Monthly Notices of the Royal Astronomical Society*, 428(4), pp.3121-3138.

Navarro, J., Frenk, C. and White, S. (1996). The Structure of Cold Dark Matter Halos. *The Astrophysical Journal*, 462, p.563.

Planck collaboration (2016). Planck 2015 results. *Astronomy & Astrophysics*, 594, p.A13.

Ponomareva, A., Verheijen, M., Papastergis, E., Bosma, A. and Peletier, R. (2017). From light to baryonic mass: the effect of the stellar mass-to-light ratio on the Baryonic Tully–Fisher relation. *Monthly Notices of the Royal Astronomical Society*, 474(4), pp.4366-4384.

Rubin, V., Thonnard, N. and Ford, W. (1980). Rotational properties of 21 SC galaxies with a large range of luminosities and radii, from NGC 4605 /R = 4kpc/ to UGC 2885 /R = 122 kpc/. *The Astrophysical Journal*, 238, p.471.

Schneider, A. (2015). Structure formation with suppressed small-scale perturbations. *Monthly Notices of the Royal Astronomical Society*, 451(3), pp.3117-3130.

Zwicky, F. (1933). Die Rotverschiebung von extragalaktischen Nebeln. *Helvetica Physica Acta,* **6**, pp.110–127

Appendix A: Selected low mass rotation curves

Here we will look at three rotation curves which were found to have low mass using the warm dark matter model and look at the full analysis or the parameters using python's emcee (Foreman-Mackey et al., 2013) and corner (Foreman-Mackey, 2016) packages.

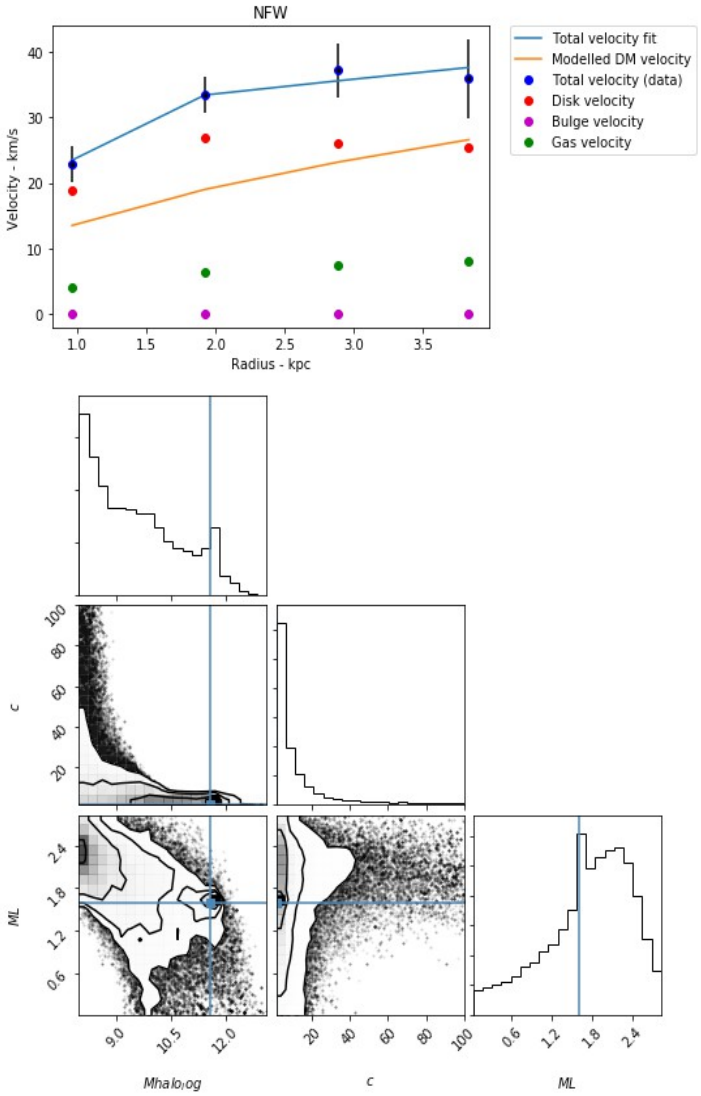

Figure A1 - D512-2 galaxy rotation curve using the NFW model

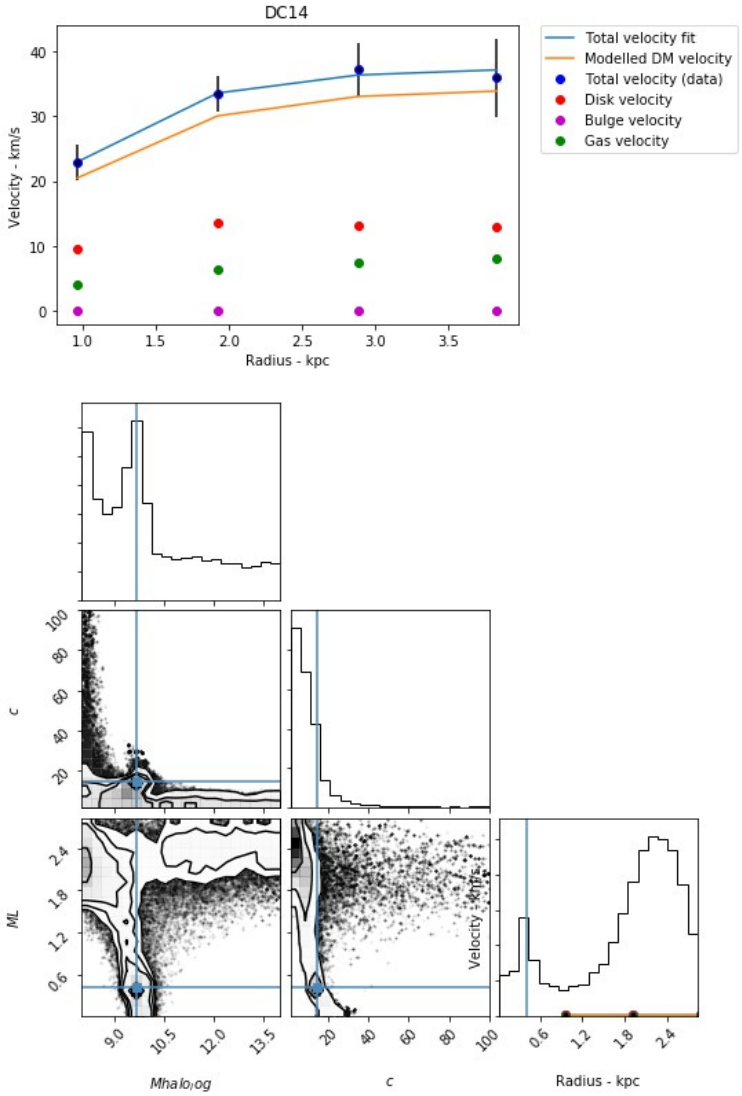

Figure A2 - D512-2 galaxy rotation curve using the DC14 model

Note that since the values of c for the warm dark matter model are a function of the halo mass the corner plots including c may not be useful or accurate.

Most noteworthy of these plots are those for UGC06628, in figures A7, A8 and A9, where the warm dark matter model is the only one to give a realistic value for the stellar mass-to-light ratio, with the DC14 model overestimating it, and suggesting that dark matter provides almost no

contribution to the total velocity of the rotation curve, and the NFW model underestimating it, suggesting that there is almost no contribution from the stars.

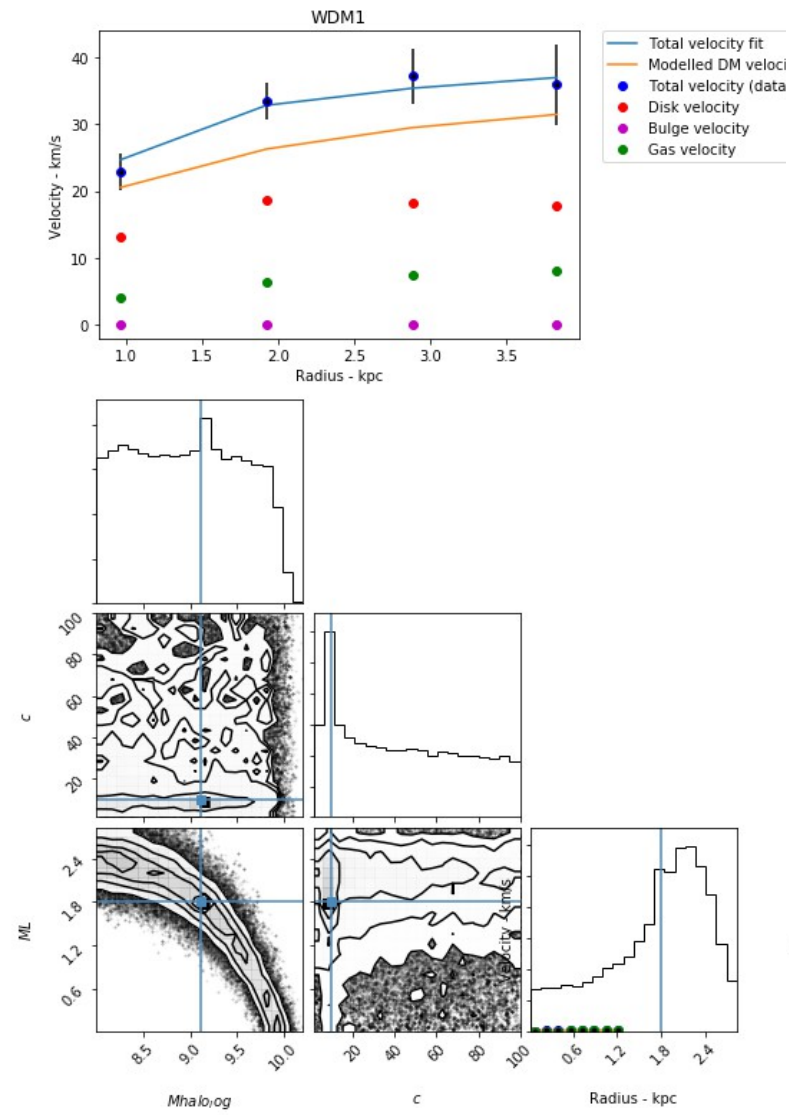

Figure A3 - D512-2 galaxy rotation curve using WDM1 mode

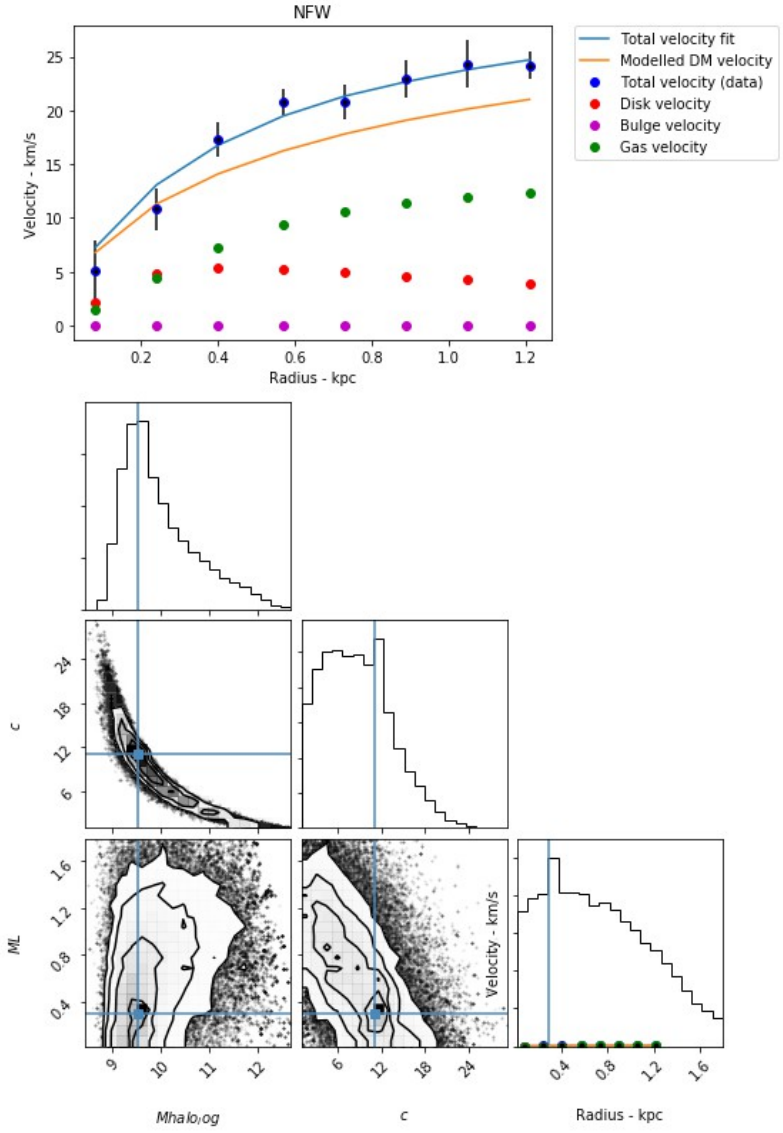

Figure A4 - UGC04483 galaxy rotation curve using NFW model

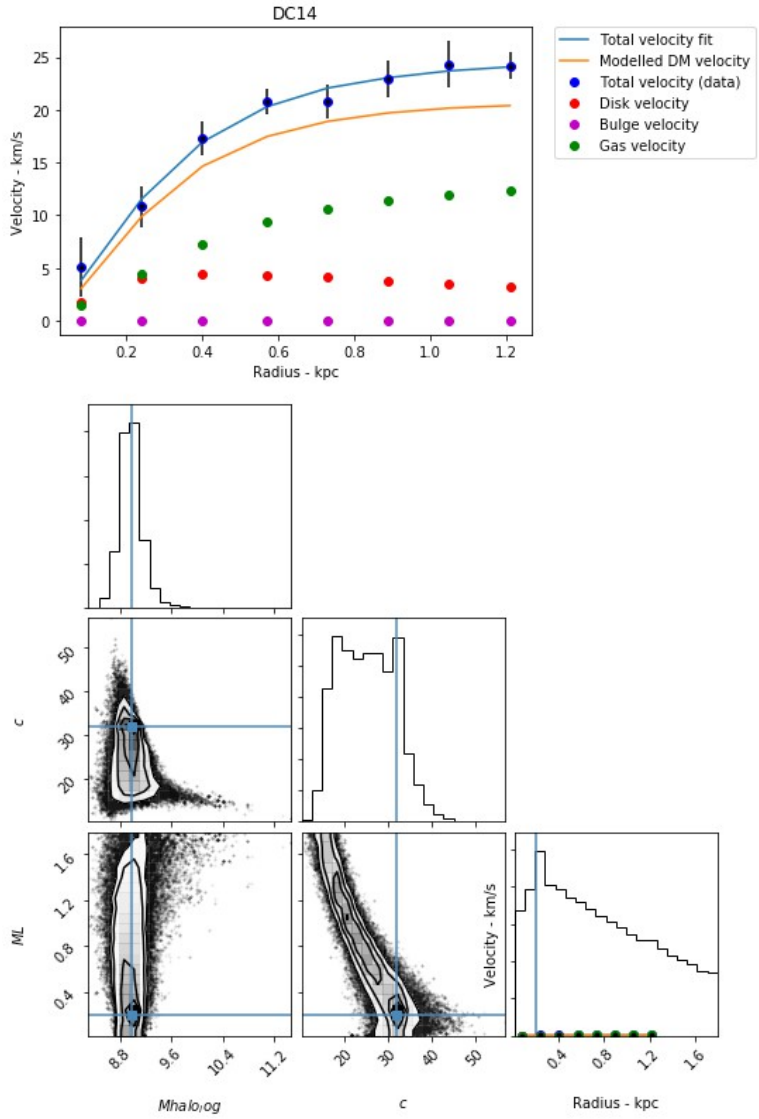

Figure A5 - UGC04483 galaxy rotation curve using the DC14 model

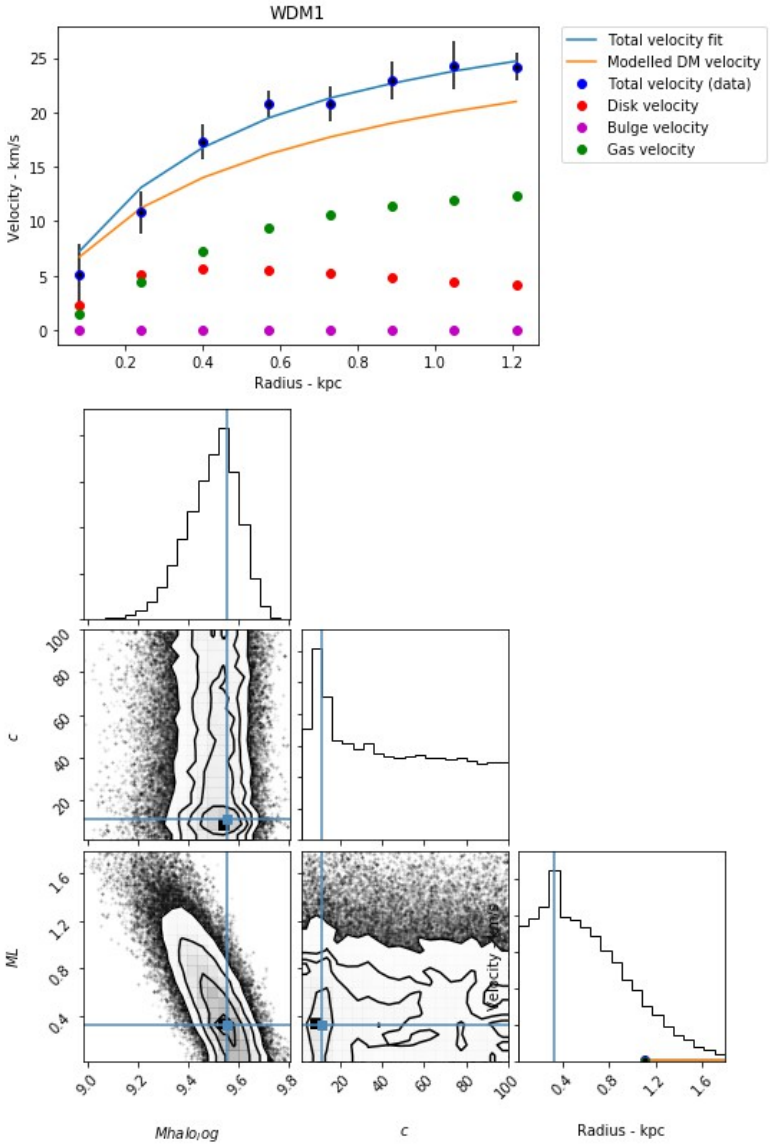

Figure A6 - UGC04483 galaxy rotation curve using the WDM1 model

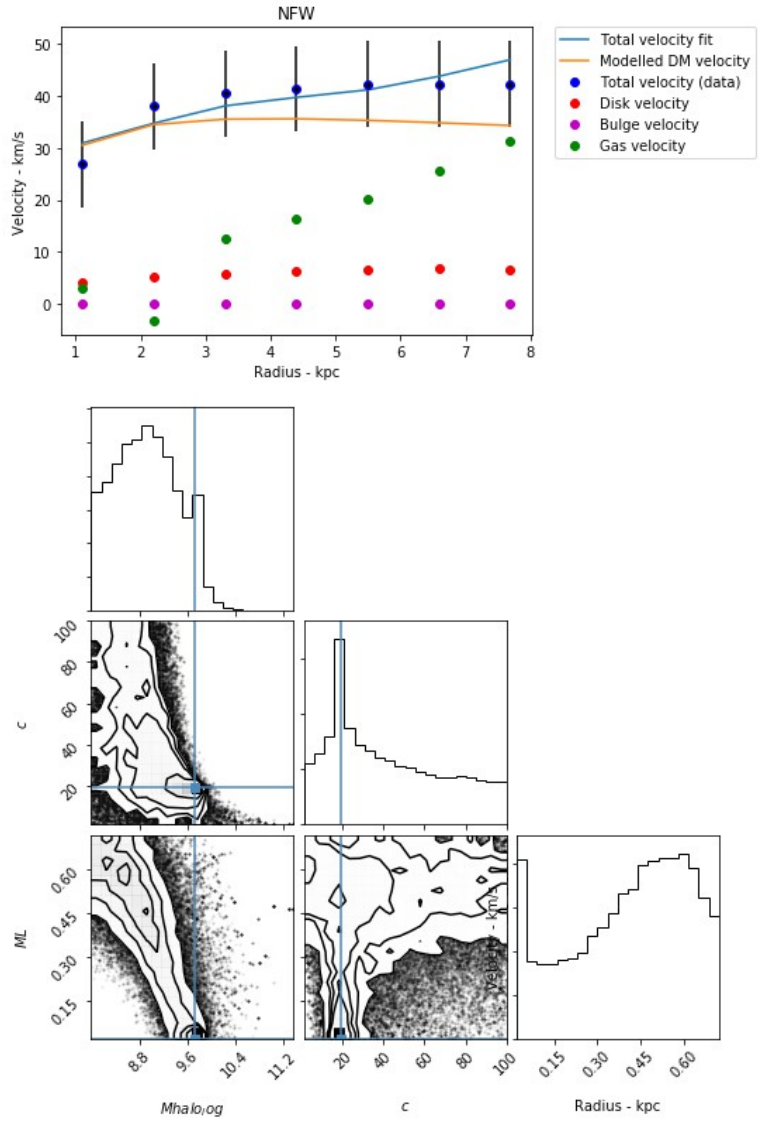

Figure A7 - UGC06628 galaxy rotation curve using the NFW model

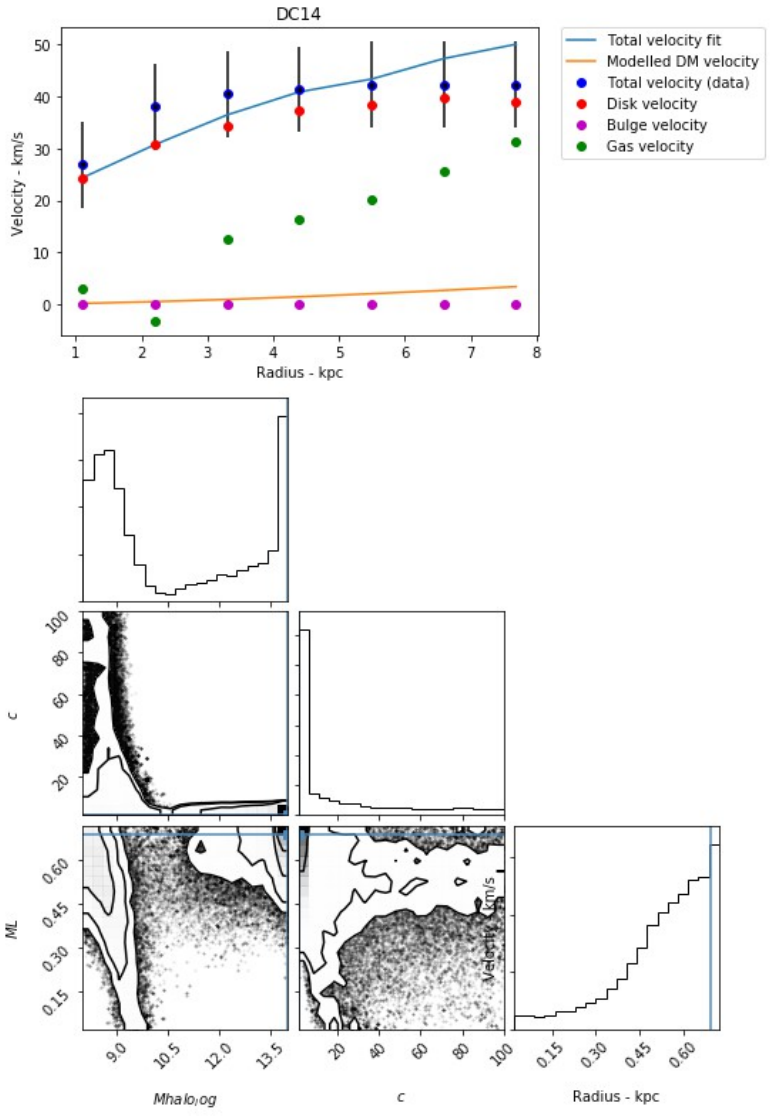

Figure A8 - UGC06628 galaxy rotation curve using the DC14 model

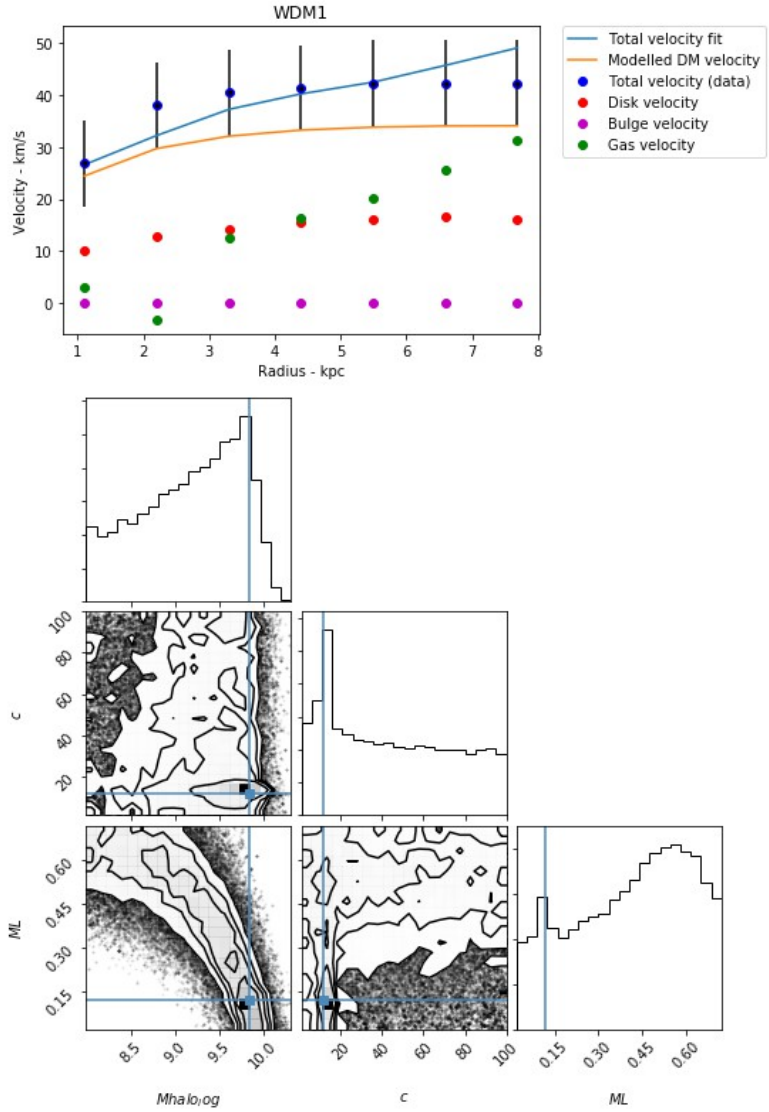

Figure A9 - UGC06628 galaxy rotation curve using the WDM1 model

Appendix B: WDM2 and WDM3 plots

Here we will show the plots for the warm dark matter models that were not included in the main report.

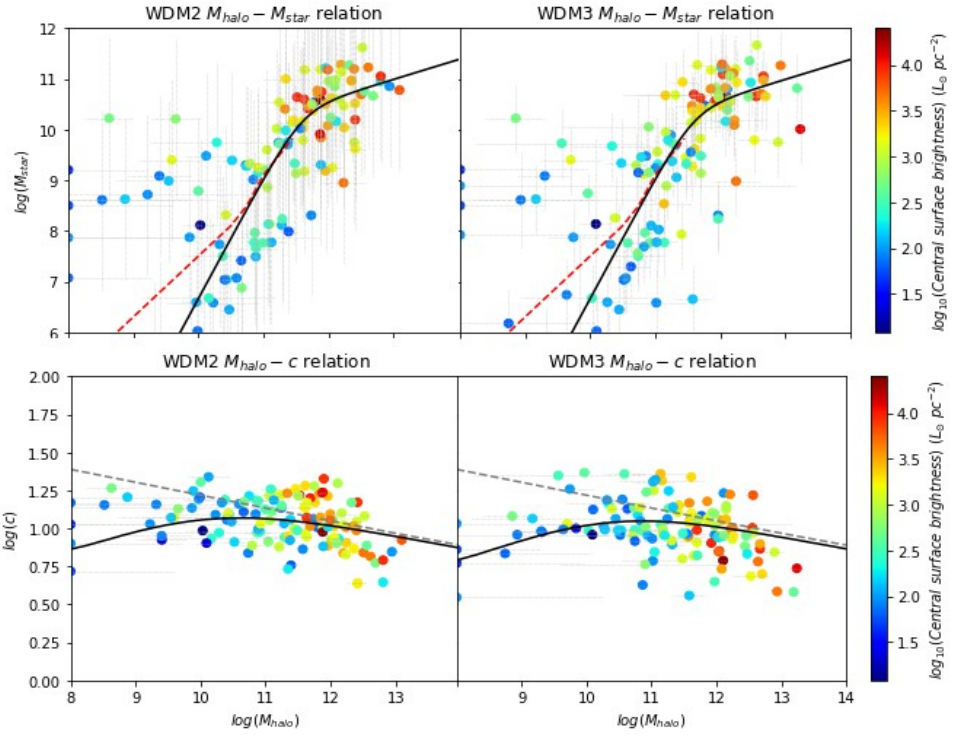

Figure B1 - The Halo mass-concentration relation and stellar mass-halo mass relation for the WDM2 and WDM3 models

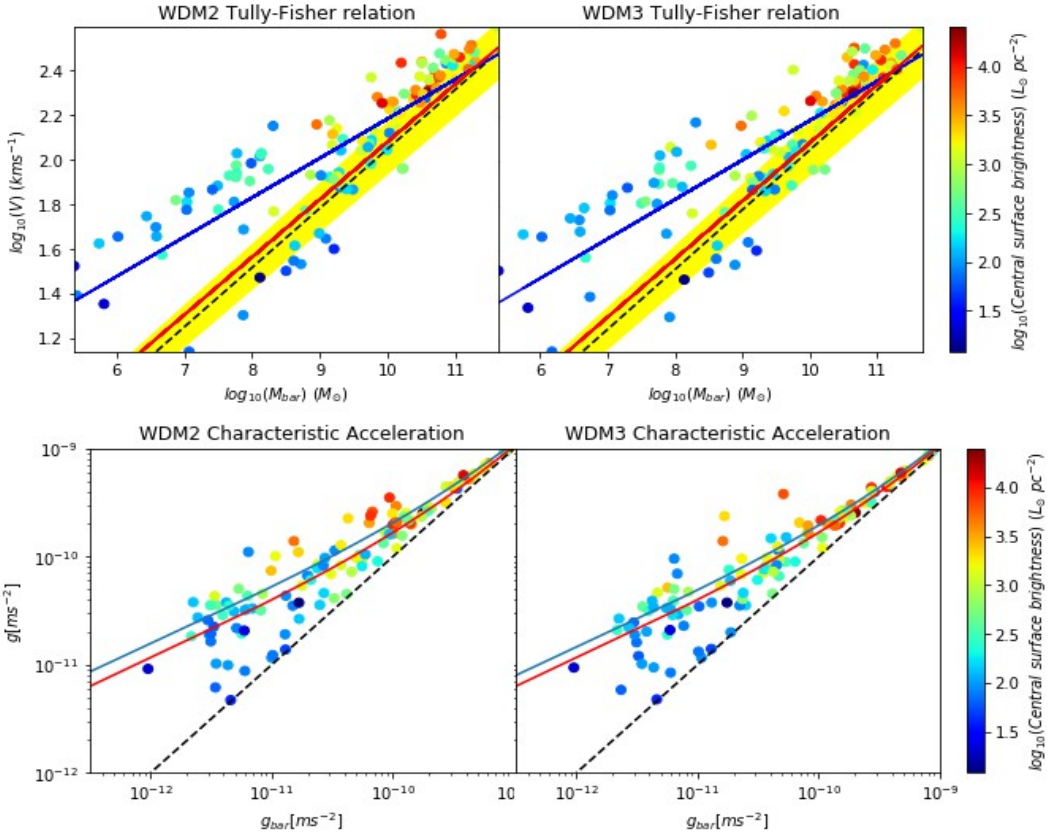

Figure B2 - The baryonic Tully-Fisher relation and the acceleration relation for the WDM2 and WDM3 models

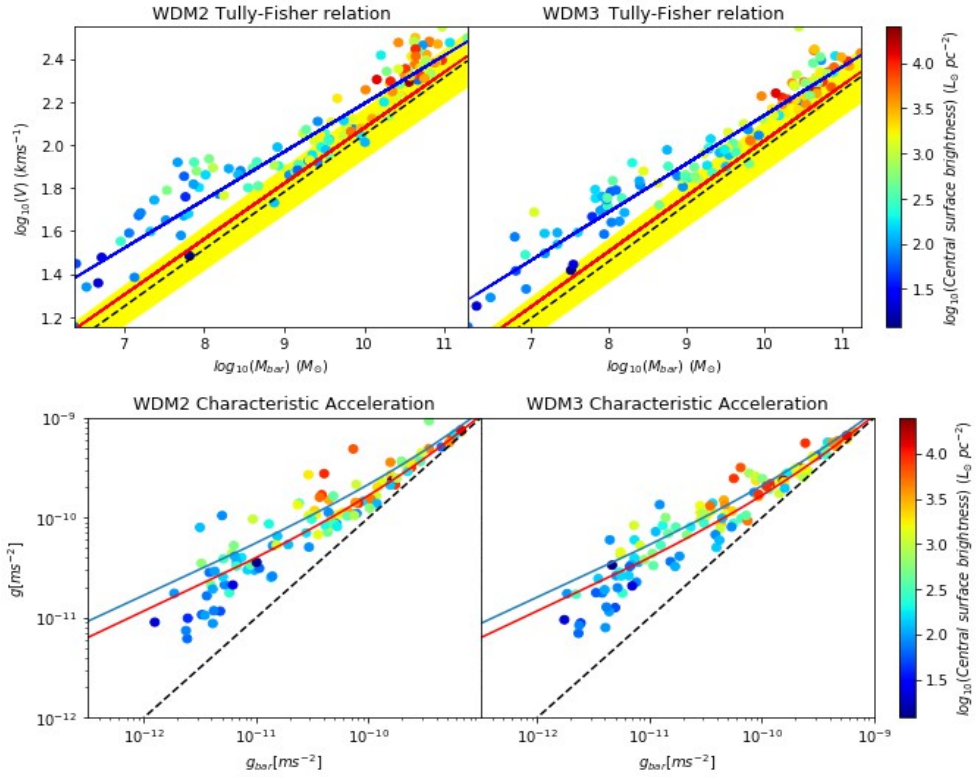

Figure B3 - The baryonic Tull-Fisher relation and acceleration relation for the WDM2 and WDM3 models using ΛCDM priors based on abundance matching

Appendix C: The Radial Acceleration Calculations

Here we will state the equations we used to find the total and baryonic accelerations for the galaxies, as well as the one used to make the theoretical prediction. For the baryonic matter:

$$g_b = \frac{V_b^2}{r} \tag{C1}$$

where g_b is the baryonic acceleration, V_b is the baryonic velocity and r is the radius. For the total acceleration:

$$g = \frac{GM_{dm}}{r^2} + \frac{V_b^2}{r} \tag{C2}$$

where g is the total acceleration and M_{dm} is the mass of the dark matter. The equation used for the theoretical predictions is:

$$g = \frac{g_b}{1 - e^{-\sqrt{g_b/g_s}}} \tag{C3}$$

where g_s is the scale acceleration parameter.